J|A|C|S ARTICLES

Published on Web 09/24/2010

Exceptional Thermal Stability in a Supramolecular Organic Framework: Porosity and Gas Storage

Wenbin Yang,[†] Alex Greenaway,[†] Xiang Lin,[†] Ryotaro Matsuda,[‡,§] Alexander J. Blake,[†] Claire Wilson,[†] William Lewis,[†] Peter Hubberstey,[†] Susumu Kitagawa,[‡,§] Neil R. Champness,*[,†] and Martin Schröder*[,†]

School of Chemistry, University of Nottingham, University Park, Nottingham, NG7 2RD, U.K., ERATO Kitagawa Integrated Pores Project, Science and Technology Agency (JST), Kyoto Research Park Building No. 3, Shimogyo-ku, Kyoto 600-8815, Japan, and Institute for Integrated Cell-Material Science (iCeMS), Kyoto University, Yoshida, Sakyo-ku, Kyoto 606-8501, Japan

Received May 18, 2010; E-mail: Neil.Champness@nottingham.ac.uk; M.Schroder@nottingham.ac.uk

Abstract: Reaction of β-amino-β-(pyrid-4-yl)acrylonitrile with the aromatic dicarboxaldehydes 9,10-bis(4-formylphenyl)anthracene and terephthalaldehyde affords the dihydropyridyl products 9,10-bis(4-((3,5-dicyano-2,6-dipyridyl)dihydropyridyl)phenyl)anthracene (L^1) and 1,4-bis(4-(3,5-dicyano-2,6-dipyridyl)dihydropyridyl)benzene (L^2), respectively. In the solid state $[L^1]\cdot 2.5DMF\cdot 3MeOH$ (**SOF-1**) crystallizes in the monoclinic space group $P2_1/c$ and forms a 3D stable supramolecular organic framework via strong $N-H\cdots N_{py}$ hydrogen bonds and $\pi-\pi$ interactions. The material incorporates pyridyl-decorated channels and shows permanent porosity in the solid state. The pore volumes of the desolvated framework **SOF-1a** calculated from the N_2 isotherm at 125 K and the CO_2 isotherm at 195 K are 0.227 and 0.244 $cm^3\ g^{-1}$, respectively. The N_2 absorption capacity of **SOF-1a** at 77 K is very low, with an uptake of 0.63 mmol g^{-1} at 1 bar, although saturation N_2 adsorption at 125 K is 6.55 mmol g^{-1} (or 143 $cm^3\ g^{-1}$). At ambient temperature, **SOF-1a** shows significant CO_2 adsorption with approximately 3 mol of CO_2 absorbed per mole of host at 16 bar and 298 K, corresponding to 69 $cm^3\ g^{-1}$ at STP. **SOF-1a** also adsorbs significant amounts of C_2H_2, with an uptake of 124 cm^3 (STP) g^{-1} (5.52 mmol g^{-1}) at 1 bar at 195 K. Methane uptake at 195 K and 1 bar is 69 cm^3 (STP) g^{-1}. Overall, gas adsorption measurements on desolvated framework **SOF-1a** reveal not only high capacity uptakes for C_2H_2 and CO_2, compared to other crystalline molecular organic solids, but also an adsorption selectivity in the order $C_2H_2 > CO_2 > CH_4 > N_2$. Overall, C_2H_2(270 K)/CH_4(273 K) selectivity is 33.7 based on Henry's Law constant, while the C_2H_2(270 K)/CO_2(273 K) ratio of uptake at 1 bar is 2.05. The less bulky analogue L^2 crystallizes in the triclinic space group $P\bar{1}$ as two different solvates $[L^2]\cdot 2DMF\cdot 5C_6H_6$ (**S2A**) and $[L^2]\cdot 2DMF\cdot 4MeOH$ (**S2B**) as pale yellow tablets and blocks, respectively. Each L^2 molecule in **S2A** participates in two $N-H\cdots O$ hydrogen bonds between dihydropyridyl rings and solvent DMF molecules. Packing of these layers generates 1D nanochannels along the crystallographic *a* and *b* axes which host DMF and benzene molecules. In **S2B**, each L^2 ligand participates in hydrogen bonding via an $N-H\cdots O$ interaction between the N−H of the dihydropyridyl ring and the O of a MeOH and also via an $N\cdots H-O$ interaction between the N center of a pyridine ring and the H−O of a second MeOH molecule. The presence of the L^2-HOMe hydrogen bonds prevents ligand−ligand hydrogen bonding. As a result, **S2B** crystallizes as one-dimensional chains rather than as an extended 3D network. Thermal removal of solvents from **S2A** results in conversion to denser phase **S2C** which shows no effective permanent porosity.

Introduction

Low-density porous organic crystalline materials (sometimes termed as "organic zeolites"[1d,e]) have attracted significant research efforts in recent years[1−7] and can be compared to porous analogues composed of metal−organic components.[8] Of particular interest is the ability of porous organic hosts to provide accessible internal surface areas for capturing, storing, and separating gases.[9,10] Such systems include crystalline covalent organic frameworks (COFs) constructed from light elements (H, B, C, N, and O) via strong covalent bonds,[1] amorphous porous organic polymers,[11] and supramolecular organic assemblies held together via weak noncovalent interactions such as hydrogen bonds and $\pi-\pi$ stacking interactions.[3c] However, since the

[†] University of Nottingham.
[‡] Science and Technology Agency (JST).
[§] Kyoto University.

(1) (a) El-Kaderi, H. M.; Hunt, J. R.; Mendoza-Cortés, J. L.; Côté, A. P.; Taylor, R. E.; O'Keeffe, M.; Yaghi, O. M. *Science* **2007**, *316*, 268. (b) Côté, A. P.; Benin, A. I.; Ockwig, N. M.; O'Keeffe, M.; Matzger, A. J.; Yaghi, O. M. *Science* **2005**, *310*, 1166. (c) Ben, T.; Ren, H.; Ma, S. Q.; Cao, D. P.; Lan, J. H.; Jing, X. F.; Wang, W. C.; Xu, J.; Deng, F.; Simmons, J. M.; Qiu, S. L.; Zhu, G. S. *Angew. Chem., Int. Ed.* **2009**, *48*, 9457. (d) Endo, K.; Koike, T.; Sawaki, T.; Hayashida, O.; Masuda, H.; Aoyama, Y. *J. Am. Chem. Soc.* **1997**, *119*, 4117. (e) Aoyama, Y. *Des. Org. Solids* **1998**, *198*, 131. (f) Aoyama, Y. *Bull. Chem. Soc. Jpn.* **2009**, *82*, 419.

Scheme 1. Views of Some of the Ligands Previously Used To Prepare Crystalline Supramolecular Organic Frameworks[a]

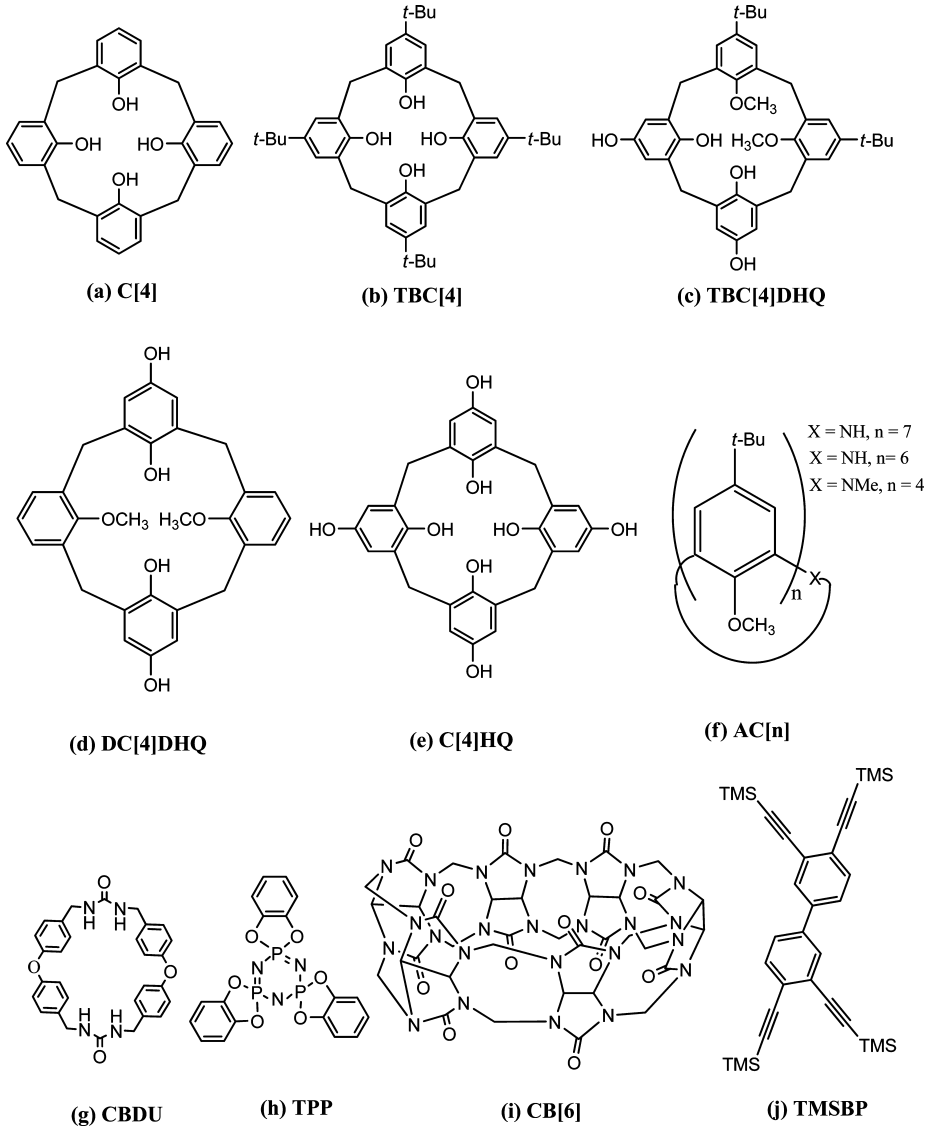

[a] (a) C[4] = calix[4]arene; (b) TBC[4] = *p-tert*-butylcalix[4]arene; (c) TBC[4]DHQ = 1,2-dimethoxy-*p-tert*-butylcalix[4]dihydroquinone; (d) DC[4]DHQ = dimethoxy-*p*-H-calix[4]dihydroquinone; (e) C[4]HQ = calix[4]hydroquinone; (f) AC[*n*] = azacalix[*n*]arene (*n* = 4, 6, 7); (g) CBDU = cyclic bis(4,4′-oxybis(benzyl))diurea; (h) TPP = tris(*o*-phenylenedioxy)cyclotriphosphazene; (i) CB[6] = cucurbit[6]uril; (j) TMSBP = 3,3′,4,4′-tetrakis(trimethylsilylethynyl)biphenyl.

removal of included species typically favors conversion to a denser phase to maximize attractive inter- and intramolecular interactions, most supramolecular organic frameworks (SOFs) are not sufficiently robust to retain microporosity upon guest removal.[2] Thus, relatively few types of SOF materials show permanent porosity with reversible gas sorption properties;[2b,3−7,10] examples of organic assemblies include anthracenebisresorcinol derivatives,[1d,e] calix[*n*]arenes (*n* = 4, 5, 6, 7),[6] dipeptides,[3] tris(*o*-phenylenedioxy)cyclotriphosphazene,[2b,12] cucurbit[6]uril (CB[6]),[10b] 3,3′,4,4′-tetra(trimethylsilylethynyl)biphenyl,[10c] and bis-urea macrocycles (Scheme 1).[10d] A common feature of these stable supramolecular organic frameworks is that they incorporate bulky building blocks with favorable molecular configurations such as hemisphere-shaped,[6c] cone-shaped,[6j] and cup-shaped,[6e,i,m] or hollowed pseudospherical shapes[10b] associated with suitable cooperative functional groups. Thus, a favorable molecular configuration promotes the formation of cavities or lattice voids, while cooperative functional groups play key roles in stabilizing molecular configurations via intramolecular[1d,6j,n] and intermolecular hydrogen bonds,[3,6n,10b] $\pi-\pi$ stacking interactions,[7a] and van der Waals forces.[6j,n]

We report herein the synthesis and assembly of the bulky dihydropyridyl tecton 9,10-bis(4-((3,5-dicyano-2,6-dipyridyl)dihy-

(2) (a) Dalgarno, S. J.; Thallapally, P. K.; Barbour, L. J.; Atwood, J. L. *Chem. Soc. Rev.* **2007**, *36*, 236. (b) Sozzani, P.; Bracco, S.; Comotti, A.; Ferretti, L.; Simonutti, R. *Angew. Chem., Int. Ed.* **2005**, *44*, 1816. (c) Maspoch, D.; Ruiz-Molina, D.; Veciana, J. *Chem. Soc. Rev.* **2007**, *36*, 770.

(3) (a) Soldatov, D. V.; Moudrakovski, I. L.; Ripmeester, J. A. *Angew. Chem., Int. Ed.* **2004**, *43*, 6308. (b) Anedda, R.; Soldatov, D. V.; Moudrakovski, I. L.; Casu, M.; Ripmeester, J. A. *Chem. Mater.* **2008**, *20*, 2908. (c) Comotti, A.; Bracco, S.; Distefano, G.; Sozzani, P. *Chem. Commun.* **2009**, 284. (d) Görbitz, C. H. *Chem.—Eur. J.* **2007**, *13*, 1022.

(4) (a) Malek, N.; Maris, T.; Perron, M.; Wuest, J. D. *Angew. Chem., Int. Ed.* **2005**, *44*, 4021. (b) Wang, X.; Simard, M.; Wuest, J. D. *J. Am. Chem. Soc.* **1994**, *116*, 12119.

(5) (a) Maspoch, D.; Domingo, N.; Ruiz-Molina, D.; Wurst, K.; Vaughan, G.; Tejada, J.; Rovira, C.; Veciana, J. *Angew. Chem., Int. Ed.* **2004**, *43*, 1828. (b) Maspoch, D.; Domingo, N.; Ruiz-Molina, D.; Wurst, K.; Tejada, J.; Rovira, C.; Veciana, J. *J. Am. Chem. Soc.* **2004**, *126*, 730.

Scheme 2. View of Structures of L^1 and L^2

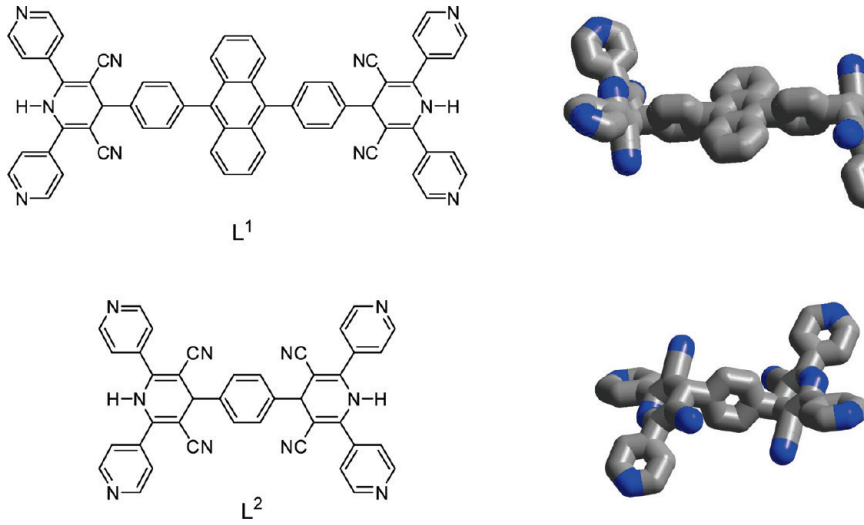

dropyridyl)phenyl)anthracene (L^1) to give a stable porous 3D network. This system combines bulky polyaromatic groups (Scheme 2), lateral nitrile, and pyridyl functional groups cojoined by dihydropyridyl moieties to afford spatially orientated hydrogen bond donor and acceptor groups. Assembly of L^1 in the solid state via hydrogen bonds and $\pi-\pi$ stacking interactions generates a porous organic framework $[L^1]\cdot 2.5DMF\cdot 3MeOH$ (**SOF-1**), showing particularly impressive thermal stability. Although MOFs can show high thermal stability and associated permanent porosity, they incorporate metals leading to an increase in the molecular weight and potential toxicity of the material. COFs and related organic materials have the advantage of light constituents but are often thermally sensitive. **SOF-1** incorporates both low molecular weight and thermal stability with permanent porosity and high gas uptake capacities and selectivity.

Experimental Section

Elemental analyses of C, H, and N were performed by the Elemental Analytical Service of the School of Chemistry, University of Nottingham, U.K. Infrared spectra were measured as KBr disks on a Nicolet Avatar 360 FT-IR system over the 4000−400 cm^{-1} range. Thermal gravimetric analysis was performed on a Rheometric Scientific STA 1500H thermal analyzer at a heating rate of 1 °C/min^{-1}. X-ray powder diffraction data were collected on a Philips X'pert powder diffractometer with Cu $K\alpha$ radiation from samples mounted on a flat glass plate sample holder. Scans of approximately 90 min were run for each sample over the range $5° \le 2\theta \le 60°$ with a step size of 0.02° in 2θ. Simulated powder patterns were generated from the final single crystal refinement model using MERCURY, version 1.4.2.[13]

Synthesis of Ligand L^1. 4-Cyanopyridine, 4-formylphenylboronic acid, potassium *tert*-butoxide, 9,10-dibromoanthracene, potassium carbonate, $Pd(PPh_3)_4$, anhydrous CH_3CN, and ZnI_2 were

(6) (a) Atwood, J. L.; Barbour, L. J.; Jerga, A.; Schottel, B. L. *Science* **2002**, *298*, 1000. (b) Ishii, Y.; Takenaka, Y.; Konishi, K. *Angew. Chem., Int. Ed.* **2004**, *43*, 2702. (c) Leontiev, A. V.; Rudkevich, D. M. *Chem. Commun.* **2004**, 1468. (d) Thallapally, P. K.; Wirsig, T. B.; Barbour, L. J.; Atwood, J. L. *Chem. Commun.* **2005**, 4420. (e) Thallapally, P. K.; Lloyd, G. O.; Wirsig, T. B.; Bredenkamp, M. W.; Atwood, J. L.; Barbour, L. J. *Chem. Commun.* **2005**, 5272. (f) Ananchenko, G. S.; Udachin, K. A.; Dubes, A.; Ripmeester, J. A.; Perrier, T.; Coleman, A. W. *Angew. Chem., Int. Ed.* **2006**, *45*, 1585. (g) Thallapally, P. K.; Lloyd, G. O.; Atwood, J. L.; Barbour, L. J. *Angew. Chem., Int. Ed.* **2005**, *44*, 3848. (h) Atwood, J. L.; Barbour, L. J.; Jerga, A. *Science* **2002**, *296*, 2367. (i) Atwood, J. L.; Barbour, L. J.; Jerga, A. *Angew. Chem., Int. Ed.* **2004**, *43*, 2948. (j) Thallapally, P. K.; McGrail, B. P.; Atwood, J. L.; Gaeta, C.; Tedesco, C.; Neri, P. *Chem. Mater.* **2007**, *19*, 3355. (k) Thallapally, P. K.; Dobrzańska, L.; Gingrich, T. R.; Wirsig, T. B.; Barbour, L. J.; Atwood, J. L. *Angew. Chem., Int. Ed.* **2006**, *45*, 6506. (l) Thallapally, P. K.; Dalgarno, S. J.; Atwood, J. L. *J. Am. Chem. Soc.* **2006**, *128*, 15060. (m) Thallapally, P. K.; McGrail, B. P.; Dalgarno, S. J.; Schaef, H. T.; Tian, J.; Atwood, J. L. *Nat. Mater.* **2008**, *7*, 146. (n) Tsue, H.; Matsui, K.; Ishibashi, K.; Takahashi, H.; Tokita, S.; Ono, K.; Tamura, R. *J. Org. Chem.* **2008**, *73*, 7748. (o) Tsue, H.; Ishibashi, K.; Tokita, S.; Takahashi, H.; Matsui, K.; Tamura, R. *Chem.—Eur. J.* **2008**, *14*, 6125.

(7) (a) Ma, B. Q.; Coppens, P. *Chem. Commun.* **2003**, 2290. (b) Bhogala, B. R.; Nangia, A. *Cryst. Growth Des.* **2003**, *3*, 547. (c) Men, Y.-B.; Sun, J.; Huang, Z.-T.; Zheng, Q.-Y. *Angew. Chem., Int. Ed.* **2009**, *48*, 2873.

(8) (a) Férey, G. *Chem. Soc. Rev.* **2008**, *37*, 191. (b) Ockwig, N. W.; Delgado-Friedrichs, O.; O'Keeffe, M.; Yaghi, O. M. *Acc. Chem. Res.* **2005**, *38*, 176. (c) James, S. L. *Chem. Soc. Rev.* **2003**, *32*, 276. (d) Murray, L. J.; Dincă, M.; Long, J. R. *Chem. Soc. Rev.* **2009**, *38*, 1294. (e) Neofotistou, E.; Malliakas, C. D.; Trikalitis, P. N. *Chem.—Eur. J.* **2009**, *15*, 4523. (f) Yang, W.; Lin, X.; Jia, J.; Blake, A. J.; Wilson, C.; Hubberstey, P.; Champness, N. R.; Schröder, M. *Chem. Commun.* **2008**, 359. (g) Wang, B.; Côté, A. P.; Furukawa, H.; O'Keeffe, M.; Yaghi, O. M. *Nature* **2008**, *453*, 207. (h) Lin, X.; Telepeni, I.; Blake, A. J.; Dailly, A.; Brown, C. M.; Simmons, J. M.; Zoppi, M.; Walker, G. S.; Thomas, K. M.; Mays, T. J.; Hubberstey, P.; Champness, N. R.; Schröder, M. *J. Am. Chem. Soc.* **2009**, *131*, 2159. (i) Yan, Y.; Lin, X.; Yang, S.; Blake, A. J.; Dailly, A.; Champness, N. R.; Hubberstey, P.; Schröder, M. *Chem. Commun.* **2009**, 1025. (j) Yang, S.; Lin, X.; Dailly, A.; Blake, A. J.; Champness, N. R.; Hubberstey, P.; Schröder, M. *Chem.—Eur. J.* **2009**, *15*, 4829. (k) Lin, X.; Jia, J.; Hubberstey, P.; Schröder, M.; Champness, N. R. *CrystEngComm.* **2007**, *9*, 438. (l) Yang, S.; Lin, X.; Blake, A. J.; Walker, G. S.; Hubberstey, P.; Champness, N. R.; Schröder, M. *Nat. Chem.* **2009**, *1*, 487. (m) Yan, Y.; Telepeni, I.; Yang, S.; Lin, X.; Kockelmann, W.; Dailly, A.; Blake, A. J.; Lewis, W.; Walker, G. S.; Allan, D. R.; Barnett, S. A.; Champness, N. R.; Schröder, M. *J. Am. Chem. Soc.* **2010**, *132*, 4092. (n) Kitagawa, S.; Kitaura, R.; Noro, S.-I. *Angew. Chem., Int. Ed.* **2004**, *43*, 2334. (o) Hinks, N. J.; McKinlay, A. C.; Xiao, B.; Wheatley, P. S.; Morris, R. E. *Microporous Mesoporous Mater.* **2010**, *129*, 330. (p) Ma, S.; Zhou, H.-C. *Chem. Commun.* **2010**, *46*, 44. (q) Li, J.-R.; Kuppler, R.; Zhou, H.-C. *Chem. Soc. Rev.* **2009**, *38*, 1477. (r) Lin, X.; Champness, N. R.; Schröder, M. *Topics in Current Chemistry*; Schröder, M., Ed.; Springer Verlag: Germany, 2010, Vol. 293, p 35.

(9) Aoyama, Y. *Top. Curr. Chem.* **1998**, *198*, 131.

(10) (a) Morris, R. E.; Wheatley, P. S. *Angew. Chem., Int. Ed.* **2008**, *47*, 4966. (b) Lim, S.; Kim, H.; Selvapalam, N.; Kim, K.-J.; Cho, S. J.; Seo, G.; Kim, K. *Angew. Chem., Int. Ed.* **2008**, *47*, 3352. (c) Msayib, K. J.; Book, D.; Budd, P. M.; Chaukura, N.; Harris, K. D. M.; Helliwell, M.; Tedds, S.; Walton, A.; Warren, J. E.; Xu, M.; McKeown, N. B. *Angew. Chem., Int. Ed.* **2009**, *48*, 3273. (d) Dewal, M. B.; Lufaso, M. W.; Hughes, A. D.; Samuel, S. A.; Pellechia, P.; Shimizu, L. S. *Chem. Mater.* **2006**, *18*, 4855.

purchased from the Aldrich Chemical Co. and used as received without further purification. 9,10-Bis(4-((3,5-dicyano-2,6-dipyridyl)dihydropyridyl)phenyl)anthracene (L^1) was synthesized from β-amino-β-(pyrid-4-yl)acrylonitrile and 9,10-bis(4-formylphenyl)-anthracene in acetic acid, with these two precursors being prepared according to previously described methods.[14]

β-Amino-β-(pyrid-4-yl)acrylonitrile (290.5 mg, 2.0 mmol) and 9,10-bis(4-formylphenyl)anthracene (193.3 mg, 0.5 mmol) were mixed in acetic acid, deaerated using N_2 for 10 min, and then heated at 125 °C to give a clear orange-red solution. After 30 min a yellow solid began to precipitate. The reaction mixture was refluxed for 48 h yielding a large amount of yellow solid, which was collected by filtration, washed with hot acetic acid, and dissolved in aqueous HCl solution (1 M, 100 mL) under heating and stirring. Basification with KOH solution to pH $\approx$ 8 afforded the deep yellow solid L^1 (yield: 348 mg, 78%).

β-Amino-β-(pyrid-4-yl)acrylonitrile, $C_8H_7N_3$. Elemental analysis (found/calcd): C, 66.15/66.19; H, 4.83/4.86; N, 28.94/28.95. IR (KBr, ν_{max}, cm^{-1}): 3335, 2193. ^1H NMR (DMSO-d_6, δ, ppm): 8.63 (d, J = 6.3 Hz, 2H), 7.57 (d, J = 6.0 Hz, 2H), 7.02 (d, 2H), 4.40 (s, 1H).

9,10-Bis(4-formylphenyl)anthracene, $C_{28}H_{18}O_2$. Elemental analysis (found/calcd): C, 87.04/87.02, H, 4.68/4.69. ^1H NMR ($CDCl_3$, δ, ppm): 10.24 (s, 2H, CHO), 8.18 (d, 4H, J = 8.2 Hz, ArH), 7.71 (d, 4H, J = 8.1 Hz, ArH), 7.65−7.61 (m, 4H, ArH), 7.42−7.39 (m, 4H, ArH). IR (KBr, ν_{max}, cm^{-1}): 1710 (CHO).

9,10-Bis(4-((3,5-dicyano-2,6-dipyridyl)dihydropyridyl)phenyl)-anthracene (L^1), $C_{60}H_{36}N_{10}$. Elemental analysis (found/calcd): C, 80.34/80.32; H, 4.05/4.03; N, 15.61/15.66. ^1H NMR (DMSO-d_6, δ, ppm): 10.44 (s, 2H, NH), 8.80 (d, J = 6.0 Hz, 8H, PyH), 7.83 (d, 4H, J = 8.1 Hz ArH), 7.77 (d, J = 6.1 Hz, 8H, PyH), 7.64−7.61 (m, 8H, ArH), 7.50−7.46 (m, 4H, ArH), and 5.08 (s, 2H, CH). IR (KBr, ν_{max}, cm^{-1}): 3417 (br), 3062 (m), 2205 (vs), 1601 (s), 1549 (m), 1510 (s), 1440 (w), 1412 (s), 1385 (m), 1290 (s), 1109 (w), 1070 (w), 828 (s), 794 (m), 611 (m) cm^{-1}.

Crystal Growth of (L^1)·2.5DMF·3MeOH (SOF-1). A hot DMF solution (5 mL) of L^1 (46.5 mg, 0.052 mmol) in a glass vial was covered with a layer of benzene (5 mL) and a further layer of MeOH (4 mL). Slow diffusion of MeOH through the benzene buffer into the DMF solution afforded a solvent mixture from which, 2 days later, yellow crystalline samples of **SOF-1** were harvested by filtration. The product was washed with benzene/MeOH and then dried in air (yield: 55.6 mg, 91%). Elemental analysis for $C_{70.5}H_{65.5}N_{12.5}O_{5.50}$ (calcd/found): C, 72.01/74.25; H, 5.61/5.01; N, 14.89/15.13. The volatility of the cocrystallized solvent in the sample contributes to the discrepancy in the elemental analysis. ^1H NMR (DMSO-d_6, δ, ppm) for **SOF-1** exposed to open air for 6 months: 10.45 (s, 2H, NH), 8.81 (d, J = 6.0 Hz, 8H, PyH), 7.96 (s, 2.5H, O=C*H*-DMF), 7.83 (d, 4H, J = 8.1 Hz ArH), 7.77 (d, J = 6.0 Hz, 8H, PyH), 7.65−7.61 (m, 8H, ArH), 7.50−7.46 (m, 4H, ArH), 5.09 (s, 2H, CH), 2.89 (s, 7.5H, *CH*$_3$-DMF), 2.73 (s, 7.5H, *CH*$_3$-DMF), corresponding to a composition of [L^1]·2.5DMF. IR (KBr, ν_{max}, cm^{-1}): 3422 (br), 3195 (s), 3079 (s), 2930 (m), 2837 (m), 2205 (s), 1660 (s), 1600 (s), 1548 (m), 1505 (s), 1438 (w), 1412 (s), 1385 (s), 1344 (m), 1291 (s), 1099 (w), 943 (w), 828 (s), 774 (m), 694 (m).

Synthesis of 1,4-Bis(4-(3,5-dicyano-2,6-dipyridyl)dihydropyridyl)-benzene (L^2 or S2C) and [L^2]·2DMF·5C_6H_6 (S2A). A solution of β-amino-β-(pyrid-4-yl)acrylonitrile (0.58 g, 4 mmol) in glacial acetic acid (15 mL) was treated with terephthalaldehyde (0.13 g, 1 mmol), and the reaction mixture was refluxed for 24 h. After the mixture was cooled to room temperature, a slightly yellow solid was isolated by filtration, washed sequentially with hot acetic acid, water, and ethanol, and dried in air (0.25 g, 38.8%). Crystals of [L^2]·2DMF·5C_6H_6 (**S2A**) and [L^2]·2DMF·4MeOH (**S2B**) were grown from a mixture of DMF−benzene−MeOH by the same layering method that was used for **SOF-1**. Elemental analysis for L^2 (or **S2C**), $C_{40}H_{24}N_{10}$ (calcd/found): C, 74.52/74.49; H, 3.75/3.71; N, 21.73/21.86. ^1H NMR (DMSO-d_6, δ, ppm): 10.41 (s, 2H, *1*-H-dihydropyridyl), 8.77 (d, J = 5.6 Hz, 8H, *2,6*-H-pyridyl), 7.65−7.71 (m, 12H, H-Ar), 4.91 (s, 2H, *4*-H-dihydropyridyl). IR (KBr, ν_{max}, cm^{-1}): 3314 (s, br), 2980 (m), 2207 (s), 1643 (s), 1599 (s), 1500 (m), 1412 (m), 1338 (m), 1290 (m), 1220 (m), 1152 (m), 1070 (m), 997 (m), 833 (m), 798 (m), 690 (m), 583 (m). Because of loss of benzene solvent at room temperature, the elemental analysis results of **S2A** were found to be variable. ^1H NMR (DMSO-d_6, δ, ppm): 10.41 (s, 2H, *1*-*H*-dihydropyridyl), 8.77 (d, 8H, J = 6.0 Hz, 2,6-*H*-pyridyl), 7.95 (s, 2H, O=C*H*-DMF), 7.65−7.71 (m, 12H, *H*-Ar), 7.36 (s, 24 H, *H*-benzene), 4.91 (s, 2H, 4-*H*-dihydropyridyl), corresponding to the composition of [L^2]·2DMF·4C_6H_6. IR (KBr, ν_{max}, cm^{-1}): 3319 (br), 3189 (m), 3084 (m), 2982 (m), 2204 (s), 1654 (s), 1597 (s), 1546 (m), 1508 (m), 1411 (s), 1387 (m), 1342 (m), 1291 (w), 1252 (m), 1151 (w), 1100 (m), 1065 (m), 998 (m), 830 (s), 734 (m), 653 (m), 582 (m), 516 (m).

X-ray Crystallographic Studies. Diffraction data from single crystals of **SOF-1**, **S2A**, **S2B**, and **S2C** were collected at 150(2) K on Bruker SMART CCD area detector diffractometers equipped with Oxford Cryosystems open-flow cryostats using graphite-monochromated Mo Kα radiation (λ = 0.710 73 Å). The structures were solved by direct methods, developed by subsequent difference Fourier syntheses, and refined using the SHELXTL software package.[15a] In **SOF-1**, one pyridine group of the ligand was disordered and this disorder was modeled as major and minor components of occupancy 0.7 and 0.3, respectively. Distance similarity restraints were applied to the pyridine ring components. In addition, C2′ had a rather high U value, almost twice that of the other atoms in the same ring. Therefore, the U value of C2′ was fixed as 0.05 $Å^2$, which is close to that of the other atoms in the same ring. A SADI restraint[15a] was applied to the disordered pyridine ring. All ordered non-H atoms were refined with anisotropic displacement parameters. All H atoms were placed in calculated positions and refined using the riding model. For **SOF-1**, PLATON/SQUEEZE[15b,c] was employed to calculate the diffraction contribution of the solvent molecules and thereby produce a set of solvent-free diffraction intensities. The final formula was calculated from the SQUEEZE results combined with elemental and TGA analytical data. Crystal and refinement data and for **SOF-1**, **S2A**, **S2B**, and **S2C** are listed in Table 1, and selected bond lengths and angles are given in Table 2. Further details of structure refinements are given in Supporting Information.

Measurements of Gas Isotherms. N_2, CO_2, and CH_4 isotherms were recorded using an IGA gravimetric adsorption apparatus at the University of Nottingham, U.K. The host sample was thermally activated by heating at 130 °C under ultrahigh vacuum (10^{-8} mbar) overnight. All isotherm data points were fitted by the IGASwin system software, version 1.03.143 (Hiden Isochema, 2004) using

(11) (a) McKeown, N. B.; Budd, P. M. *Chem. Soc. Rev.* **2006**, *35*, 675. (b) Mastalerz, M. *Angew. Chem., Int. Ed.* **2008**, *47*, 445. (c) Wood, C. D.; Tan, B.; Trewin, A.; Su, F.; Rosseinsky, M.; Bradshaw, D.; Sun, Y.; Zhou, L.; Cooper, A. I. *Adv. Mater.* **2008**, *20*, 1916. (d) Campbell, N. L.; Clowes, R.; Ritchie, L. K.; Cooper, A. I. *Chem. Mater.* **2009**, *21*, 204. (e) Tozawa, T.; Jones, J. T. A.; Swamy, S. I.; Jiang, S.; Adams, D. J.; Shakespeare, S.; Clowes, R.; Bradshaw, D.; Hasell, T.; Chong, S. Y.; Tang, C.; Thompson, S.; Parker, J.; Trewin, A.; Bacsa, J.; Slawin, A. M. Z.; Steiner, A.; Cooper, A. I. *Nat. Mater.* **2009**, *8*, 973.

(12) (a) Sozzani, P.; Comotti, A.; Simonutti, R.; Meersmann, T.; Logan, J. W.; Pines, A. *Angew. Chem., Int. Ed.* **2000**, *39*, 2695. (b) Couderc, G.; Hertzsch, T.; Behrnd, N. R.; Kramer, K.; Hulliger, J. *Microporous Mesoporous Mater.* **2006**, *88*, 170. (c) Hertzsch, T.; Gervais, C.; Hulliger, J.; Jaeckel, B.; Guentay, S.; Bruchertseifer, H.; Neels, A. *Adv. Funct. Mater.* **2006**, *16*, 268.

(13) Nolze, G.; Kraus, W. *Powder Diffr.* **1998**, *13*, 256. (b) http://www.ccdc.cam.ac.uk/ products/mercury.

(14) (a) Teki, Y.; Miyamoto, S.; Nakatsuji, M.; Miura, Y. *J. Am. Chem. Soc.* **2001**, *123*, 294. (b) Yamagushi, Y.; Katsuyama, I.; Funabiki, K.; Matsui, M.; Shibata, K. *J. Heterocycl. Chem.* **1998**, *35*, 805.

(15) (a) Sheldrick, G. M. *Acta Crystallogr., Sect. A* **2008**, *64*, 112. (b) Spek, A. L. *PLATON, Acta Crystallogr., Sect. D* **2009**, *65*, 148. (c) Sluis, P. v. d.; Spek, A. L. *Acta Crystallogr., Sect. A* **1990**, *46*, 194.

Table 1. Crystal Data and Structure Refinement for **SOF-1**, **S2A**, **S2B**, and **S2C**

	compound				
parameter	$[L^1]\cdot 2.5DMF\cdot 3MeOH$ (**SOF-1**)	$[L^2]\cdot 2DMF\cdot 5C_6H_6$ (**S2A**)	$[L^2]\cdot 2DMF\cdot 5C_6H_6$ (**S2A**)	$[[L^2]\cdot 2DMF\cdot 4MeOH$ (**S2B**)	L^2 (**S2C**)
chemical formula	$C_{70.5}H_{65.5}N_{12.5}O_{5.50}$	$C_{76}H_{68}N_{12}O_2$	$C_{76}H_{68}N_{12}O_2$	$C_{50}H_{54}N_{12}O_6$	$C_{40}H_{24}N_{10}$
FW	1175.85	1181.42	1181.42	919.05	644.699
crystal size (mm^3)	0.31 × 0.21 × 0.12	0.37 × 0.34 x0.10	0.49 × 0.18 x0.16	0.22 × 0.22 x0.20	0.21 × 0.17 × 0.07
space group	$P2_1/c$	$P\bar{1}$	$P\bar{1}$	$P\bar{1}$	$P2_1/n$
a (Å)	14.319(2)	8.3803(9)	8.3720(14)	9.0709(7)	10.617(3)
b (Å)	6.8536(8)	12.1013(12)	12.087(2)	10.9421(8)	13.214(4)
c (Å)	32.694(4)	16.1017(16)	16.072(3)	12.7964(10)	11.835(3)
α (deg)	90	87.352(2)	87.336(3)	93.573(1)	90
β (deg)	93.782(2)	88.209(2)	88.089(3)	99.335(1)	91.952(6)
γ (deg)	90	79.709(2)	79.577(3)	104.496(1)	90
V ($Å^3$)	3201.5(7)	1604.5(3)	1597.3(5)	1206.32(16)	1659.4(14)
ρ_{calcd} (g/cm^3)	1.220	1.223	1.228	1.265	1.290
θ_{min}, θ_{max} (deg)	2.79, 27.49	2.09, 27.54	2.18, 27.19	2.36, 27.53	2.3, 26.85
μ (mm^{-1})	0.080	0.076	0.076	0.086	0.081
F(000)	1240	624	624	486	668
no. of reflns	19894	14190	14285	8696	9679
no. of unique reflns	7876	7163	7146	5190	3922
no. of paras	309	408	409	382	226
R_{int}	0.069	0.058	0.0227	0.0244	0.053
R,[a] R_w[b]	0.0783, 0.188	0.0419, 0.1048	0.0499, 0.1273	0.0487, 0.113	0.082, 0.162
GOF[c]	0.854	1.019	1.031	1.046	1.01
max/min residuals (e $Å^{-3}$)	0.40/−0.29	0.25/−0.17	0.45/−0.19	0.29/ −0.20	0.31/−0.28

[a] $R = \sum|F_o| - |F_c|/\sum|F_o|$. [b] $R_w = [\sum w(F_o^2 - F_c^2)^2/\sum w(F_o^2)^2]^{1/2}$. [c] GOF = $\{\sum[\ w(F_o^2 - F_c^2)^2]/(n-p)\}^{1/2}$.

Scheme 3. Synthesis of L^1 and L^2 [a]

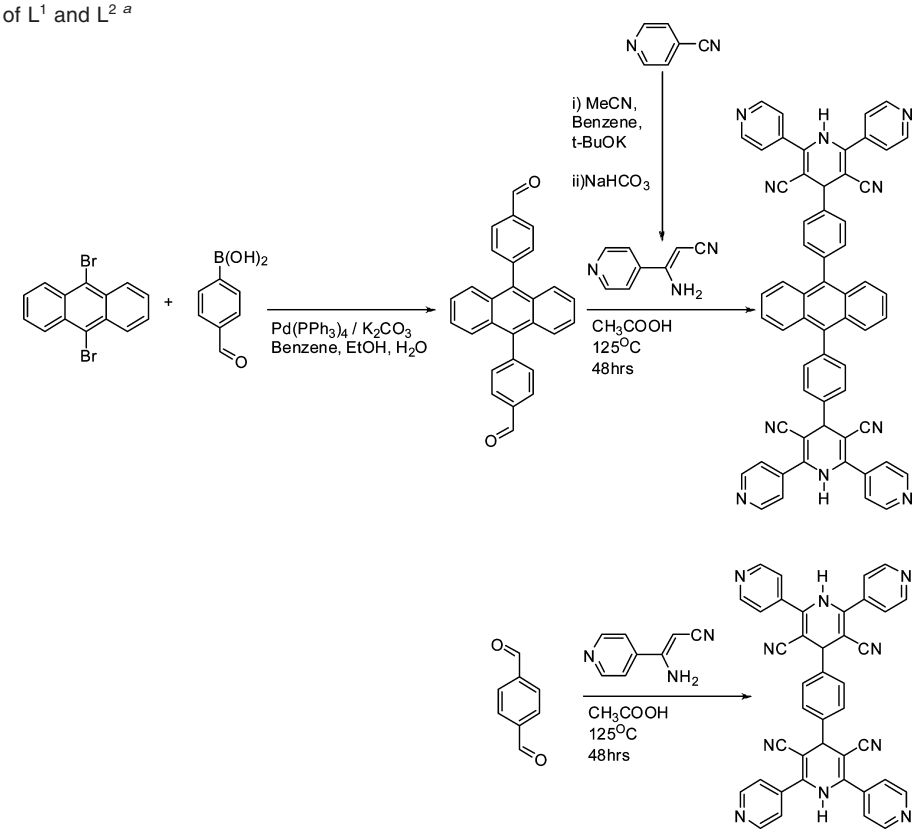

[a] Precursors 9,10-bis(4-formylphenyl)anthracene and β-amino-β-(pyrid-4-yl)acrylonitrile were prepared according to previously described methods.[14]

a linear driving force model when >98% equilibration had been reached. The adsorption isotherms of acetylene at various temperatures were measured with BELSORP-max volumetric adsorption equipment from Bel Japan, Inc. Acetylene gas of high purity (>99.9999%) was used. The host sample was treated under reduced pressure ($<10^{-3}$ Pa) at 400 K for more than 12 h before each measurement. Measurement temperatures were precisely controlled by a closed helium cycle refrigerator based cryostat. Each point in the adsorption isotherm has an uncertainty of ±0.25% imposed by the resolution of the pressure gauge.

Results and Discussion

Structure of SOF-1. The polypyridyl tecton L^1 was synthesized from β-amino-β-(pyrid-4-yl)acrylonitrile and 9,10-bis(4-formylphenyl)anthracene in acetic acid (Scheme 3). Crystalli-

Table 2. Selected Bond Lengths (Å) and Angles (deg) and Hydrogen Bond Data for [L^1]·2.5DMF·3MeOH **(SOF-1)**, [L^2]·2DMF·5C_6H_6 (**S2A**), [L^2]·2DMF·4MeOH (**S2B**), and L^2 (**S2C**)

SOF-1

N(1)−C(5)	1.342(5)	C(8)−C(18)	1.521(3)	C(20)−C(21)	1.382(4)	C(1)−N(1)−C(5)	116.6(5)
C(1)−C(2)	1.373(5)	C(9)−C(17)	1.425(4)	C(21)−C(22)	1.385(4)	C(2)−C(3)−C(4)	119.7(4)
C(3)−C(4)	1.377(5)	C(10)−C(11)	1.487(3)	C(24)−C(25)	1.398(4)	N(1)−C(5)−C(4)	123.7(5)
C(3)−C(6)	1.534(5)	N(3)−C(13)	1.345(3)	C(26)−C(27)	1.361(4)	C(10)−N(2)−C(6)	121.4(2)
C(4)−C(5)	1.387(5)	C(11)−C(15)	1.387(4)	C(27)−C(28)	1.409(4)	C(6)−C(7)−C(16)	120.0(3)
N(2)−C(6)	1.384(3)	N(4)−C(17)	1.136(4)	C(28)−C(30)#1	1.353(4)	C(7)−C(8)−C(18)	111.2(2)
C(6)−C(7)	1.370(3)	C(18)−C(23)	1.389(4)	C(29)−C(30)	1.439(4)	C(7)−C(8)−H(8A)	108.5
C(8)−C(9)	1.520(3)	C(19)−C(20)	1.387(4)	C(29)−C(25)#1	1.440(4)	N(4)−C(17)−C(9)	177.9(3)

D−H···A	*d*(D−H)	*d*(H···A)	*d*(D···A)	∠(DHA)
N(2)−H(2B)···N(3)#2	0.86	2.03	2.873(3)	164.9
C(2)−H(2A)···N(5)#3	0.93	2.50	3.362(5)	154.2
C(8)−H(8A)···N(5)#4	0.98	2.63	3.529(4)	153.1
C(19)−H(19A)···N(4)#5	0.93	2.54	3.300(4)	139.6
C(23)−H(23A)···N(5)#4	0.93	2.63	3.371(4)	136.7

symmetry code: (#1) $-x+3, -y+1, -z$; (#2) $-x+2, y+{}^1/_2, -z-{}^1/_2$; (#3) $-x+2, -y+1, -z$; (#4) $-x+2, -y, -z$; (#5) $x, y+1, z$

S2A

N(1)−C(5)	1.3365(18)	C(6)−C(7)	1.3830(19)	C(12)−C(13)	1.5270(17)	C(14)−C(13)−C(12)	108.36(10)
N(1)−C(1)	1.3415(18)	C(7)−C(8)	1.3910(18)	C(13)−C(14)	1.5248(16)	C(14)−C(13)−C(18)	112.77(10)
C(2)−C(3)	1.3931(17)	N(3)−C(15)	1.3760(15)	N(5)−C(17)	1.1496(16)	C(12)−C(13)−C(18)	111.45(10)
N(2)−C(10)	1.3395(19)	C(12)−C(16)	1.4321(17)	C(18)−C(20)	1.3932(17)		

D−H···A	*d*(D−H)	*d*(H···A)	*d*(D···A)	∠(DHA)
N(3)−H(3A)···O(1)	0.88	1.91	2.7795(14)	170.6
C(22)−H(22B)···N(4)#1	0.98	2.60	3.424(2)	142.1
C(29)−H(29A)···N(1)#2	0.95	2.53	3.433(2)	159.9

symmetry code: (#1) $x, y-1, z$; (#2) $-x+1, -y, -z$

S2B

N(1)−C(5)	1.336(2)	C(6)−C(3)	1.4834(18)	N(3)−C(11)	1.335(2)	C(2)−C(3)−C(6)	120.00(12)
N(1)−C(1)	1.337(2)	C(7)−C(16)	1.432(2)	C(11)−C(12)	1.385(2)	C(10)−N(2)−C(6)	121.07(12)
C(1)−C(2)	1.381(2)	C(7)−C(8)	1.5278(18)	C(12)−C(13)	1.3916(19)	C(7)−C(6)−N(2)	120.75(12)
C(2)−C(3)	1.3926(19)	C(8)−C(9)	1.5253(19)	C(14)−C(15)	1.382(2)	C(6)−C(7)−C(16)	120.34(12)
C(3)−C(4)	1.391(2)	C(8)−C(18)	1.5308(19)	C(16)−N(4)	1.1462(19)	C(9)−C(8)−C(7)	107.98(11)
C(4)−C(5)	1.385(2)	C(9)−C(10)	1.353(2)	C(17)−N(5)	1.146(2)	C(7)−C(8)−C(18)	112.04(11)
N(2)−C(10)	1.3719(17)	C(9)−C(17)	1.427(2)	C(18)−C(20)	1.3850(19)	C(9)−C(8)−H(8A)	108.3
C(6)−C(7)	1.3538(19)	C(10)−C(13)	1.4890(19)	C(19)−C(20)#1	1.389(2)	N(4)−C(16)−C(7)	176.79(15)

D−H···A	*d*(D−H)	*d*(H···A)	*d*(D···A)	∠(DHA)
N(2)−H(2B)···O(1)	0.88	1.97	2.8526(16)	178.7
O(1)−H(1B)···N(3)#2	0.84	1.94	2.7695(16)	169.8
O(3)−H(3A)···O(2)	0.84	1.97	2.780(6)	162.8

symmetry code: (#1) $-x, -y+2, -z$; (#2) $-x, -y+1, -z+1$

S2C

N(1)−C(1)	1.331(7)	C(3)−C(4)	1.382(5)	C(9)−C(10)	1.343(4)	C(7)−C(8)−C(9)	108.7(3)
N(2)−C(10)	1.376(4)	C(4)−C(5)	1.392(5)	C(10)−C(11)	1.479(4)	C(7)−C(8)−C(18)	110.4(3)
N(3)−C(13)	1.330(5)	C(6)−C(7)	1.343(5)	C(11)−C(15)	1.380(4)	C(9)−C(8)−C(18)	112.8(3)
N(4)−C(16)	1.135(5)	C(7)−C(8)	1.510(5)	C(11)−C(12)	1.390(4)	C(7)−C(8)−H(8A)	108.3
N(5)−C(17)	1.140(5)	C(8)−C(9)	1.514(5)	C(12)−C(13)	1.383(5)	N(4)−C(16)−C(9)	174.4(4)
C(1)−C(2)	1.377(7)	C(8)−C(18)	1.530(4)	C(18)−C(19)	1.373(4)	N(5)−C(17)−C(7)	174.4(7)

D−H···A	*d*(D−H)	*d*(H···A)	*d*(D···A)	∠(DHA)
N(2)−H(2B)···N(3)#1	0.88	2.43	3.206(4)	148
C(5)−H(5A)···N(5)#2	0.95	2.41	3.327(7)	162

symmetry code: (#1) $-x, -y, -z$; (#2) $x-{}^1/_2, -y-{}^1/_2, z-{}^1/_2$

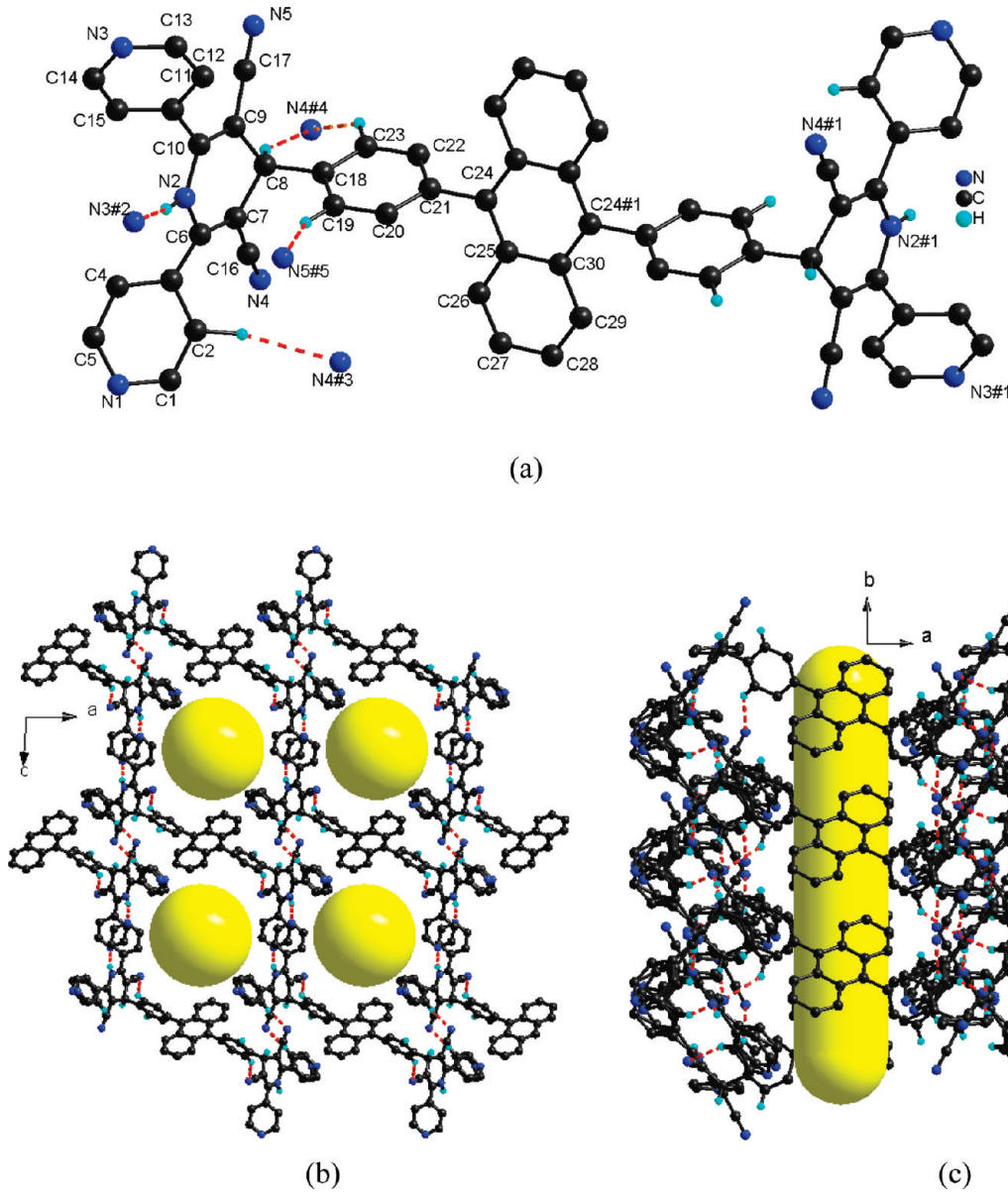

Figure 1. Crystal structure of **SOF-1**. (a) View of the molecular structure of L^1 and hydrogen bonding for the symmetric unit in **SOF-1**. Symmetry codes are as follows: (1) $-x+3, -y+1, -z$; (2) $-x+2, y+{}^1/_2, -z-{}^1/_2$; (3) $-x+2, -y+1, -z$; (4) $-x+2, -y, -z$; (5) $x, y+1, z$. (b) View of 3D supramolecular organic framework of **SOF-1**. (c) Side view of the nanochannel in **SOF-1**. Color codes are as follows: C, dark gray; H, green; N, blue; covalent bonds, dark solid lines; hydrogen bonds, red dashed lines (H atoms not involved in hydrogen bonds are omitted for clarity).

zation of L^1 affords an unprecedented supramolecular organic framework with a composition of $L^1 \cdot 2.5DMF \cdot 3MeOH$ (**SOF-1**), which crystallizes in the monoclinic space group $P2_1/c$ with two molecules of L^1 per unit cell. The structure of **SOF-1** shows L^1 lying across a crystallographic inversion center, which is coincident with the centroid of the anthracene moiety, and comprises two 3,5-dicyano-2,6-dipyridyldihydropyridyl units bridged by the 9,10-bis(phenyl)anthracene moiety (Figure 1a). X-ray diffraction analysis confirms that C8 in the dihydropyridyl ring (C6−C7−C8−C9−C10−N2) has a sp^3 configuration, and consequently the dihydropyridyl rings are nearly perpendicular to the phenyl spacer (dihedral angle: 82.36°) and have a dihedral angle of 71.76° with respect to the central anthracene moiety. This defined geometry (Scheme 2) coupled to functional centers affords extensive hydrogen bonding between the two N−H protons and eight proton-acceptor N-sites and $\pi-\pi$ stacking interactions between the molecular building units. Each molecule of L^1 thus participates in the construction of three different hydrogen bonded motifs, strong $N-H\cdots N_{pyridyl}$ and weak $C-H\cdots N_{pyridyl}$ and $C-H\cdots N_{cyano}$, resulting in a 3D supramolecular organic framework structure with pyridyl-functionalized channels along the *b* axis. These channels have a diameter of ~7.8 Å (Figure 1b). Further $\pi-\pi$ stacking interactions between the molecular building units along the *b* axis contribute further to the stabilization of the overall network. The solvent-accessible voids were estimated using PLATON/VOID[15b] to be 34.0% of the total crystal volume, giving a calculated density of 0.93 g cm^3 g^{-1} for the desolvated organic framework.

High Thermal Stability of SOF-1. Thermogravimetric analysis (TGA) of **SOF-1** reveals (Figure 2) a rapid weight loss of 23.33% up to 175 °C, corresponding to thermal removal of three MeOH and 2.5 DMF molecules (calculated weight loss 23.68%), followed by a wide plateau region. The major weight loss starting beyond 420 °C corresponds to decomposition of the material. The thermal stability of **SOF-1** is quite remarkable, much higher than that of organic framework materials reported

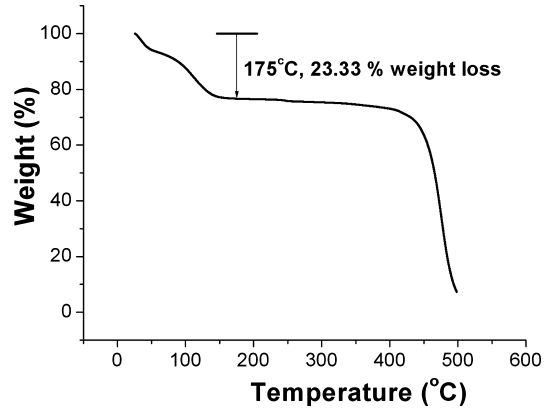

Figure 2. TGA trace for [L^1]·2.5DMF·3MeOH (**SOF-1**).

previously[2−7] and comparable to thermally stable metal−organic frameworks.[16] It appears that the presence of a large aromatic spacer, 9,10-bis(phenyl)anthracene, and strong N−H···N_{py} hydrogen bonds play an important role in stabilizing the guest-free framework of **SOF-1a**. It is noteworthy that the fully evacuated framework (**SOF-1a)**, which was obtained by heating a crystalline sample of **SOF-1** at 130 °C under a dynamic ultrahigh vacuum (10^{-8} mbar) for 12 h, remains structurally unchanged on desolvation, as confirmed by powder X-ray diffraction studies, producing nanospace for accommodation of other guest molecules. **SOF-1a** has the formula $C_{60}H_{36}N_{10}$ (L^1), as confirmed by elemental analysis and ^{1}H NMR spectroscopic data.

Effect of Aromatic Ring on Thermal Stability and Porosity. To study the effect of the aromatic spacer on the stability and porosity of the resultant material, we synthesized the less bulky analogue 1,4-bis(4-(3,5-dicyano-2,6-dipyridyl)dihydropyridyl)-benzene (L^2). By use of the same layering techniques applied to **SOF-1** (L^1), it is possible to obtain L^2 as crystalline materials. Two different crystalline solvates of L^2, solvate A [L^2]·2DMF·$5C_6H_6$ (**S2A**) and solvate B [L^2]·2DMF·4MeOH (**S2B**), were obtained. **S2A** and **S2B** both crystallize in the triclinic space group $P\bar{1}$ as pale yellow tablets and slightly yellow blocks, respectively. Each L^2 molecule in **S2A** participates in two N−H···O hydrogen bonds between dihydropyridyl rings and solvent DMF molecules. These terminal DMF molecules prevent the dicyanodipyridyldihydropyridyl moiety from participating in additional hydrogen bonds. However, the crystal structure features $\pi-\pi$ stacking interactions between pyridyl rings to form a 2D layered assembly with $\pi-\pi$ stacked columns of ligands. Packing of these layers generates 1D nanochannels along the crystallographic *a* and *b* axes which host DMF and benzene molecules (Figure 3). In **S2B**, each L^2 ligand participates in hydrogen bonding via an N−H···O interaction between the N−H of the dihydropyridyl ring and the O of a MeOH molecule, with N···H−O hydrogen bonding between the N-center of a pyridine ring and the H−O of a second MeOH molecule. The presence of the L^2−HOMe hydrogen bonds prevents ligand−ligand hydrogen bonding, and there are no $\pi-\pi$ stacking interactions between pyridyl moieties. As a result, **S2B** crystallizes as one-dimensional hydrogen bonded chains rather than as an extended 3D network (Figure 4).

Although analysis using PLATON/VOID[15b] suggests the possibility of a high solvent-accessible volume of 57.9%, **S2A** undergoes a transformation to a denser phase **S2C** upon thermal removal of solvents at 160 °C under N_2. Indeed, this transformation also occurs on exposure to air where crystals of **S2A** gradually convert to **S2C** at room temperature, as revealed by PXRD studies. **S2C** crystallizes in the monoclinic space group $P2_1/n$ and has a 3D supramolecular network featuring strong N−H···N_{py} and weak C−H···N_{cyano} bonds and $\pi-\pi$ contacts (Figure 5). However, **S2C** does not exhibit any evidence of microporosity, since the removal of solvent molecules from **S2A** results in conversion to the denser phase **S2C**. In addition to the role of hydrogen bonding and $\pi-\pi$ interactions, hydrophobic and van der Waals interactions between the walls of the channel host and guest molecules will also play a role in stabilizing the structure of **SOF-1**, and these weak, isotropic interactions will be far fewer in the **S2** series because of their much smaller linker group thus leading to more close-packed structures.

Gas Adsorption Properties of SOF-1a. The high stability of the organic framework **SOF-1** provides an opportunity to study its gas adsorption properties. Desolvated **SOF-1a** shows significant CO_2 adsorption at 195 K (Figure 6) especially at low

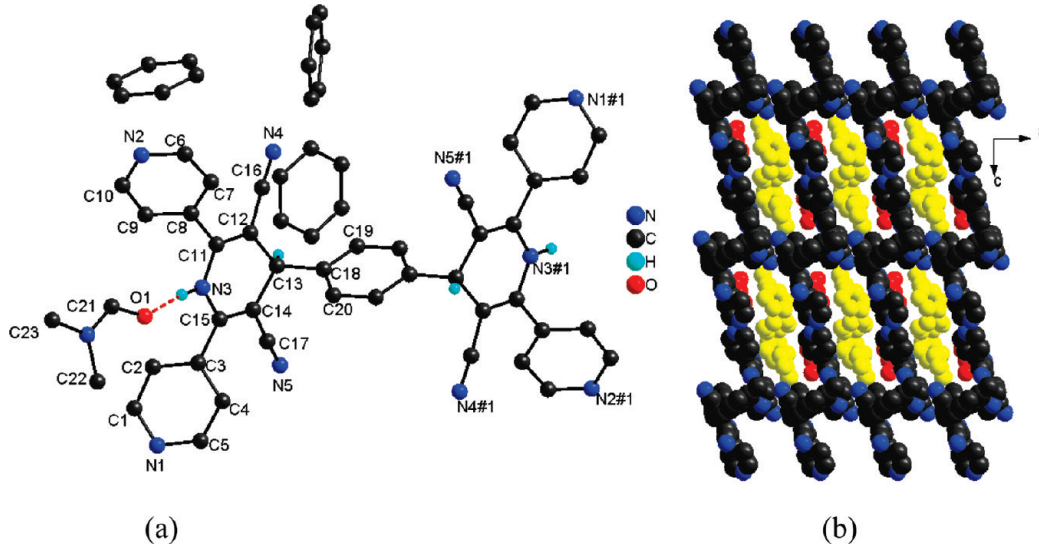

Figure 3. (a) View of molecular structure and hydrogen bonds in [L^2]·2DMF·$5C_6H_6$ (**S2A**). (b) A space-filling view of the 3D supramolecular framework of **S2A** with nanochannels capturing DMF (red) and benzene molecules (yellow). Color codes are as follows: C, black; N, blue. H atoms are omitted for clarity.

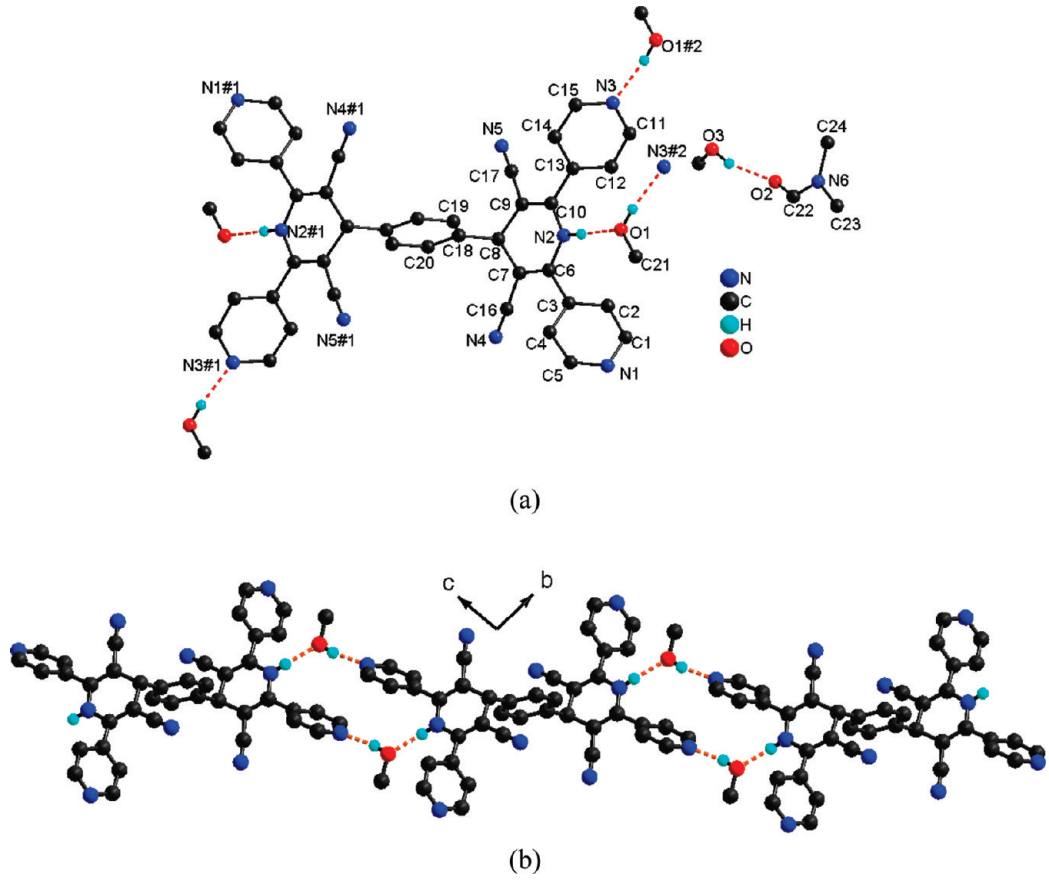

Figure 4. (a) View of asymmetric unit and hydrogen bonds in $[L^2]\cdot 2DMF\cdot 4MeOH$ (**S2B**). (b) View of the 1D chain in **S2B**, formed by L^2 and MeOH molecules via N−H···O and O−H···N bonds. H atoms on carbons are omitted for clarity.

relative pressures (3.9 mmol g^{-1} at $P = 0.2$ bar), confirming the presence of permanent microporosity. The CO_2 absorption follows a type-I isotherm,[17] with a measured capacity of 5.6 mmol g^{-1} (24.6 wt % or 125 cm^3 (STP) g^{-1}) and an estimated maximum filling of 6.5 mmol g^{-1} (28.5 wt % or 145 cm^3 (STP) g^{-1}), significantly exceeding the capacities previously reported for other supramolecular organic frameworks (Table 3).[2b,3c,6j,n] Even at ambient temperature, evacuated **SOF-1a** still shows a noticeable CO_2 adsorption with some 3 mol of CO_2 absorbed per mole of host at 16 bar and 298 K, corresponding to 69 cm^3 g^{-1} at STP. This value, which does not represent full capacity, is already effectively twice that of TBC[4]DHQ (35 cm^3 g^{-1} at 35 bar and 298 K) previously described as the most effective molecular organic assembly for absorbing CO_2.[6j]

In contrast, the N_2 absorption capacity of **SOF-1a** at 77 K is very low with only 0.63 mmol g^{-1} uptake at 1 bar, indicating that N_2 molecules are unable to enter the pores. This sorption behavior may be due to the low thermal energy of the framework and the low kinetic energy of N_2,[8p,q,18] because the results at 125 K and upward are quite different to those at 77 K. The saturation N_2 adsorption at 125 K is 6.55 mmol g^{-1} (or 143 cm^3 g^{-1}), 10 times greater than that measured at 77 K. As expected, adsorption equilibrium was achieved far more rapidly than at 77 K. The pore volumes of **SOF-1a** calculated from the N_2 isotherm at 125 K and the CO_2 isotherm at 195 K are 0.227 and 0.244 cm^3 g^{-1}, respectively. These values are relatively low compared to MOFs[8,16] and COFs[1,19] but are significant for molecular organic solids (Table 3).[3−6] The pore size (7.4 Å) obtained by applying the Dubinin−Astakhov (DA)[20] equation to the N_2 sorption data at 125 K is consistent with the crystal structure. The amount of N_2 adsorbed then reduces on increasing temperature, with uptakes at 20 bar of 6.36, 4.37, and 2.46 mmol g^{-1} at 125, 175, and 195 K, respectively.

Adsorption isotherms for C_2H_2 uptake were measured at different temperatures (Figure 6). **SOF-1a** adsorbs a significant amount of C_2H_2 at 195 K, with an uptake of 124 cm^3 (STP) g^{-1} (5.52 mmol g^{-1}) at 1 bar. With increasing temperature, the adsorption of C_2H_2 gradually decreases but becomes more reversible. The amounts of C_2H_2 adsorbed at 1 bar at 210, 230, 250, and 270 K are 104, 87, 72, and 61 cm^3 g^{-1}, respectively. When these values are fitted to the double-exponential-decay expression

$$n = n_0 + A_1\exp(-T/b_1) + A_2\exp(-T/b_2)$$

where n is absorbed amount, T is temperature (K), and n_0, A_1, A_2, b_1, and b_2 are coefficients, the amount of adsorbed C_2H_2

(16) (a) Humphrey, S. M.; Chang, J. S.; Jhung, S. H.; Yoon, J. W.; Wood, P. T. *Angew. Chem., Int. Ed.* **2007**, *46*, 272. (b) Perles, J.; Iglesias, M.; Martin-Luengo, M.-A.; Monge, M. A.; Ruiz-Valero, C.; Snejko, N. *Chem. Mater.* **2005**, *17*, 5837. (c) Lin, X.; Blake, A. J.; Wilson, C.; Sun, X.; Champness, N. R.; George, M. W.; Hubberstey, P.; Mokaya, R.; Schröder, M. *J. Am. Chem. Soc.* **2006**, *128*, 10745. (d) Sun, D.; Ma, S.; Ke, Y.; Petersen, T. M.; Zhou, H.-C. *Chem. Commun.* **2005**, 2663.

(17) Rouquerol, J.; Rouquerol, F.; Sing, K. W. *Adsorption by Powders and Porous Solids: Principles, Methodology and Applications*; Academic Press: London, 1999.

(18) Chandler, B. D.; Cramb, D. T.; Shimizu, G. K. H. *J. Am. Chem. Soc.* **2006**, *128*, 10403.

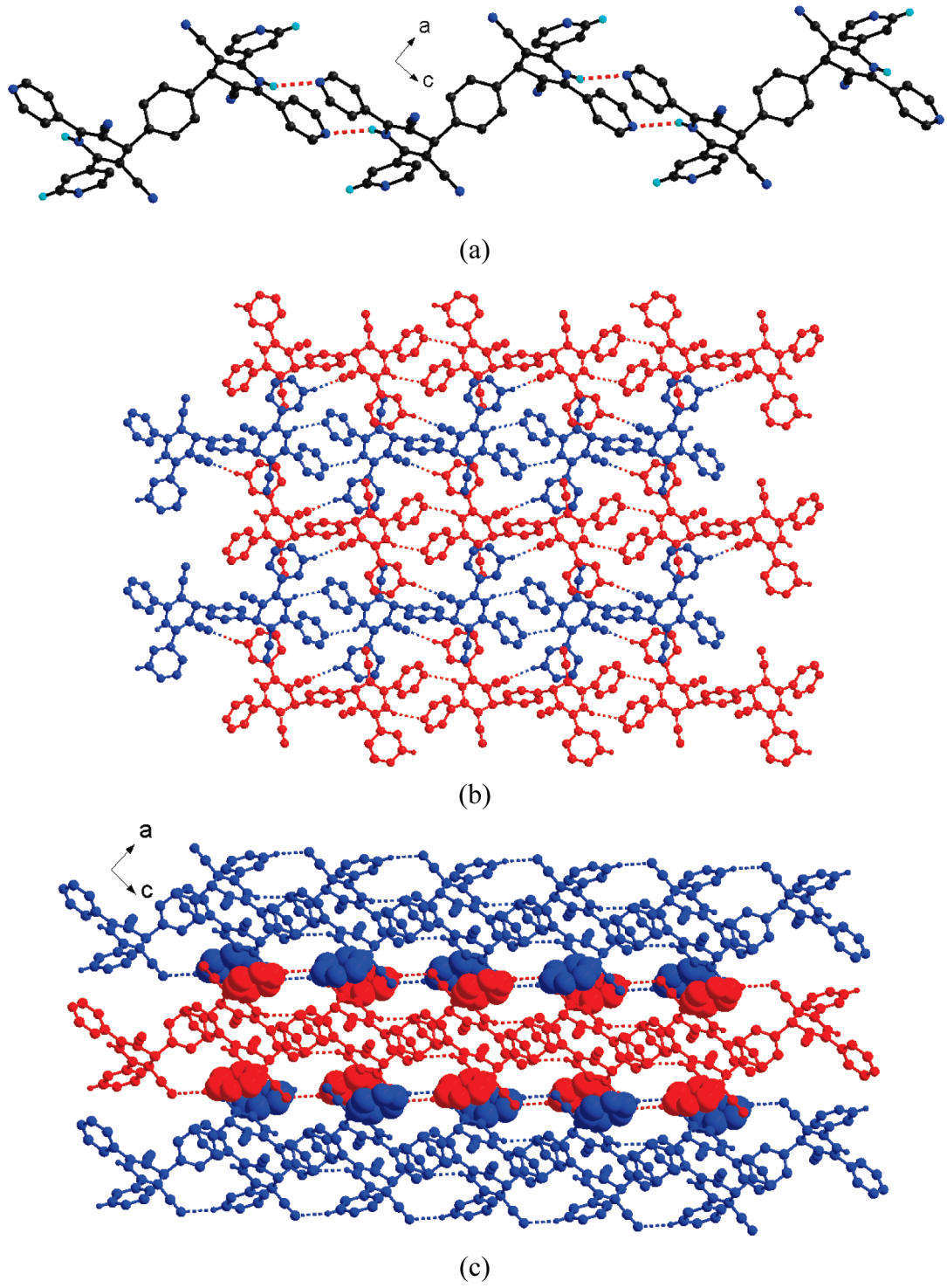

Figure 5. (a) View of L^2 molecules in **S2C** are connected via N−H···$N_{pyridyl}$ bonds into 1D supramolecular chains. (b) View of 2D supramolecular sheet in **S2C** (adjacent 1D chains highlighted with different colors, viewed along [1, 0, −1] direction). (c) View of $\pi-\pi$ contacts connecting these supramolecular layers into a 3D network (adjacent layers highlighted with different colors, $\pi-\pi$ stacking interactions between layers highlighted in space-filling mode; viewed along *b* axis). Hydrogen bonds are shown as dashed lines.

above 270 K can be estimated as 50 $cm^3\ g^{-1}$ at 298 K and 48 $cm^3\ g^{-1}$ at 303 K. These values are comparable or superior to the C_2H_2 uptakes reported for other microporous adsorbents under similar conditions (298 K and 1 atm) (Table 4).[6k,10b,21]

SOF-1a shows methane uptake at 195 K and 1 bar of 69 cm^3 (STP) g^{-1}, exceeding that of organic absorbents such as tris-*o*-phenylenedioxycyclotriphosphazene (33.2 cm^3 (STP) g^{-1}),[2b] L-alanyl-L-valine (50 cm^3 (STP) g^{-1}) and L-valyl-L-alanine (35 cm^3 (STP) g^{-1})[3c] under similar conditions (195 K and 1 atm) (Table 5). When the pressure of CH_4 is increased to 10 bar, the amount adsorbed is 106 cm^3 (STP) g^{-1}, but this does not represent its full capacity. The CH_4 uptake significantly

(19) (a) Han, S. S.; Furukawa, H.; Yaghi, O. M.; Goddard, W. A. *J. Am. Chem. Soc.* **2008**, *130*, 11580. (b) Furukawa, H.; Yaghi, O. M. *J. Am. Chem. Soc.* **2009**, *131*, 8875.
(20) Dubinin, M.-M. *Carbon* **1989**, *27*, 457.

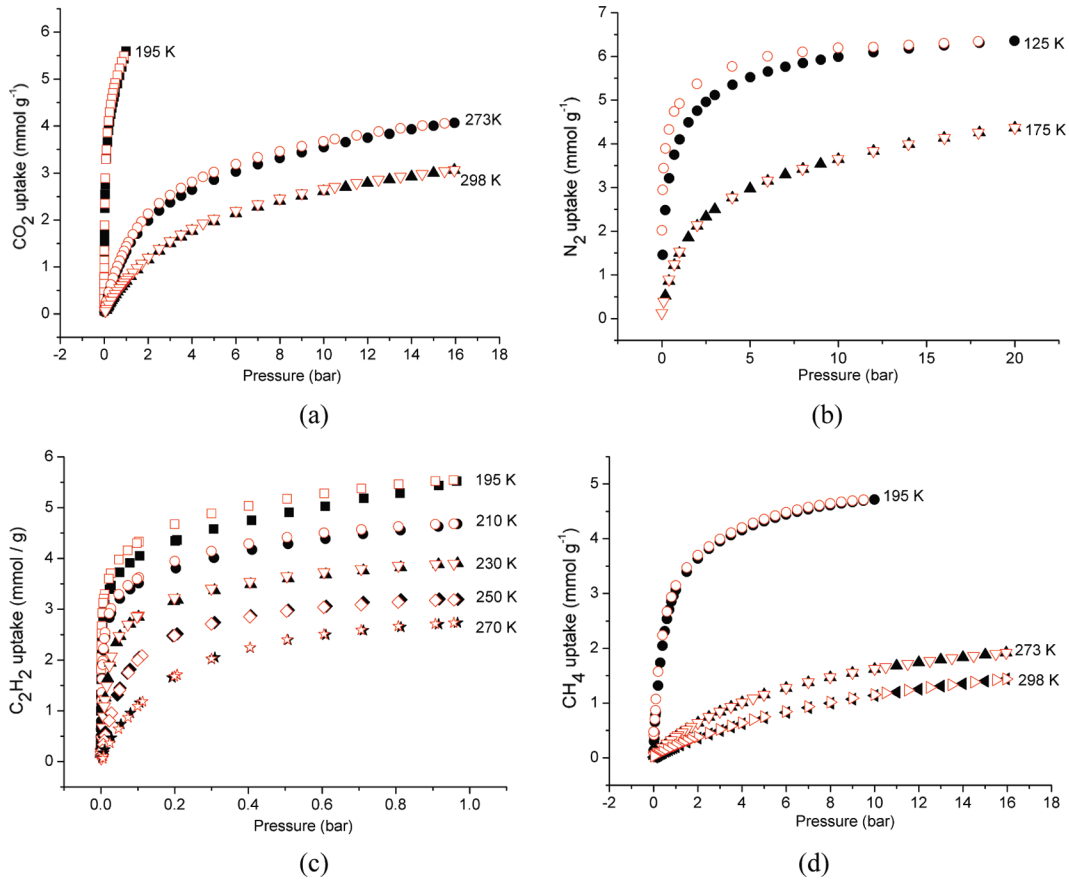

Figure 6. Gas isotherms for **SOF-1a**: (a) CO_2 at 195, 273, and 298 K; (b) N_2 at 125 and 175 K; (c) C_2H_2 at 195, 210, 230, 250, and 270 K; (d) CH_4 at 195, 270, and 298 K. Black solid symbols indicate adsorption, and red open symbols indicate desorption.

Table 3. Comparison of N_2 and CO_2 Sorption Data for Supramolecular Organic Frameworks (SOFs)

		S_A, m^2 g^{-1}			V (CO_2) [cm^3 g^{-1}]		
material[a]	V (N_2)[b] [cm^3 g^{-1}]	BET[d]	Langmuir[d]	V(N_2)[c] [cm^3 g^{-1}]	195 K[h]	298 K	ref
SOF-1a	143[c]	474[e]	639[e] (671)[f]	0.227[e,g] (0.244)[f,g]	125	16[h] (69)[i]	this work
TBC[4]DHQ	90	230		0.14		35[i]	6j, 10c
TPP	55		240	0.088	61		2b, 10b
CB[6]	85	210		0.13			10b
TMSBP	98	278		0.16			10c
CBDU		341[f]			72		10d
VA					91		3c
AV					78		3c
AC[6]					37		6o
AC[7]					55		6n

[a] Molecular structures and corresponding abbreviations are shown in Scheme 1. TBC[4]DHQ = *p-tert*-butylcalix[4]dihydroquinone; TPP = tris-*o*-phenylenedioxycyclotriphosphazene; CB[6] = cucurbit[6]uril; TMSBP = 3,3′,4,4′-tetra(trimethylsilylethynyl)biphenyl; VA = L-valyl-L-alanine; AV = L-alanyl-L-valine; CBDU = cyclic bis(4,4′-oxybis(benzyl))diurea; AC[6] = azacalix[6]arene; AC[7] = azacalix[7]arene. [b] Amount of nitrogen adsorbed at 77 K and 1 atm except where indicated. [c] Amount of nitrogen adsorbed at 125 K and 1 bar. [d] Calculated from N_2 isotherm at 77 K except where indicated. [e] Calculated from N_2 isotherm at 125 K. [f] Calculated from CO_2 isotherm at 195 K. [g] $\rho(N_2, 77K) = 0.808$ g cm^{-3} and $\rho(CO_2$, at triple point) = 1.18 g cm^{-3} were applied to calculate the pore volume. [h] Amount of CO_2 adsorbed at 1 atm or 1 bar. [i] Amount of CO_2 adsorbed at 16 bar. [j] Amount of CO_2 adsorbed at 35 atm.

decreases with increasing temperature, but the density of adsorbed CH_4 (0.09 g cm^{-3} at 298 K and 16 bar) is still comparable to the values reported for COFs (0.06− 0.13 g cm^{-3} at 298 K and 35 bar).[19b]

(21) (a) Matsuda, R.; Kitaura, R.; Kitagawa, S.; Kubota, Y.; Belosludov, R. V.; Kobayashi, T. C.; Sakamoto, H.; Chiba, T.; Takata, M.; Kawazoe, Y.; Mita, Y. *Nature* **2005**, *426*, 238. (b) Samsonenko, D. G.; Kim, H.; Sun, Y.; Kim, G.-H.; Lee, H.-S.; Kim, K. *Chem.—Asian J.* **2007**, *2*, 484. (c) Zhang, J.-P.; Chen, X.-M. *J. Am. Chem. Soc.* **2009**, *131*, 5516. (d) Zhang, J.-P.; Kitagawa, S. *J. Am. Chem. Soc.* **2008**, *130*, 907. (e) Xiang, S.; Zhou, W.; Gallegos, J. M.; Liu, Y.; Chen, B. *J. Am. Chem. Soc.* **2009**, *131*, 12415. (f) Reid, C. R.; Thomas, K. M. *Langmuir* **1999**, *15*, 3206.

High Selectivity of Gas Adsorption on SOF-1a. It is interesting to compare the adsorption properties of **SOF-1a** toward different gases at the same temperatures. At 195 K, the absorption of C_2H_2 at 200 mbar reaches 4.3 mmol g^{-1} (75% maximum loading); even at pressures as low as 50 mbar the absorption is still extremely efficient (Figure 7). In contrast, the adsorption of CH_4 with increasing pressure presents a significantly smaller slope, and the C_2H_2/CH_4 ratios thus become greatly advantageous below 50 mbar, reaching values as high as 18. However, from a practical application point of view, it is critical to be able to achieve separation of C_2H_2 from CH_4 at ambient temperature and normal pressure. The C_2H_2 uptake at 1 bar and

Table 4. Comparison of Acetylene Sorption in Porous Supramolecular Organic Frameworks (SOFs)

material[a]	C_2H_2 uptake ($cm^3\ g^{-1}$) at 1 atm or 1 bar: 195 K	270 K	298 K	Q_{st} (kJ mol^{-1})	ref
SOF system					
SOF-1a	124	61	50[b]	36.2[d](43.3)[e]	this work
CB[6]	91		52	59.4[e]	10b
TBC[4]			18		6k
carbon molecular sieve			45[c]		20

[a] Abbreviations: CB[6] = cucurbit[6]uril; TBC[4] = *p-tert*-butylcalix[4]arene. [b] Estimated by fitting the acetylene absorbed amounts at 1 bar at different temperatures (195, 210, 230, 250, and 270 K) to a double-exponential-decay equation. [c] V_{ads} (STP) at 303 K. [d] Calculated from the adsorption isotherms at 230, 250, and 270 K by using virial method 2 at zero coverage. [e] Calculated by using the Clausius−Clapeyron equation at low coverage.

Table 5. Comparison of CH_4 Sorption in Porous Supramolecular Organic Frameworks (SOFs)

material[a]	CH_4 uptake, $cm^3\ g^{-1}$: 195 K[b]	298 K[d]	CH_4 density,[g] g cm^{-3}	Q_{st}, kJ mol^{-1}	ref
SOF					
SOF-1a	69, 106[c]	32[e]	0.09	23.76[h] (20.84)[i]	this work
TPP	33				12b
TBC[4]		24			6d
TPC[4]		31[f]			6d
VA	50			9[i]	3c
AV	35			9[i]	3c
IV	40			19[i]	3c

[a] TPP = tris-*o*-phenylenedioxycyclotriphosphazene; TBC[4] = *p-tert*-butylcalix[4]arene; TPC[4] = *p-tert*-pentylcalix[4]arene; VA = L-valyl-L-alanine; AV = L-alanyl-L-valine; IV = L-isoleucyl-L-valine. [b] V_{ads} (STP) at 195 K and 1 atm (or 1 bar) except where indicated. [c] V_{ads} (STP) at 195 K and 10 bar. [d] V_{ads} (STP) at 35 bar or 35 atm, room temp, except where indicated. [e] V_{ads} (STP) at 298 K and 16 bar. [f] V_{ads} (STP) at 32 atm, room temp. [g] Calculated density of adsorbed CH_4 at room temp in pore volume (V_p). [h] Estimated by a modified version of the Clausius−Clapeyron equation at low coverage (0.1 mmol g^{-1}). [i] Estimated by virial method.

270 K is 2.75 mmol g^{-1}, while the CH_4 uptake under the similar conditions (1 bar and 273 K) is 0.38 mmol g^{-1}. To calculate the C_2H_2(270 K)/CH_4(273 K) selectivity from the corresponding Henry's Law constants, a nonlinear fitting of the adsorption isotherms was performed using the Tóth model.[8e] Accordingly, the Henry's Law selectivity of C_2H_2 over CH_4 is calculated to be 33.7, indicating a significantly stronger interaction of C_2H_2 molecules with the host framework (possibly due to polar pyridyl groups in the pores) compared to CH_4.

At 195 K, the C_2H_2/CO_2 ratios are 1.09 ± 0.07 between 0.1 and 1 bar, indicating low adsorption selectivity. However, the superiority of C_2H_2 adsorption over CO_2 adsorption is apparent at near ambient temperature and up to atmospheric pressure (Figure 7b). The calculated Henry's Law selectivity of C_2H_2(270 K) over CO_2(273 K) is 6.02, while the C_2H_2(270 K)/CO_2(273 K) ratio of uptake at 1 bar is 2.05, significantly higher than the values for those of carbon molecular sieves (1.25),[21f] TBC[4] (1.25),[6k] and MOFs (1.34−1.48),[21a−e] suggesting that **SOF-1a** can distinguish these gas molecules.

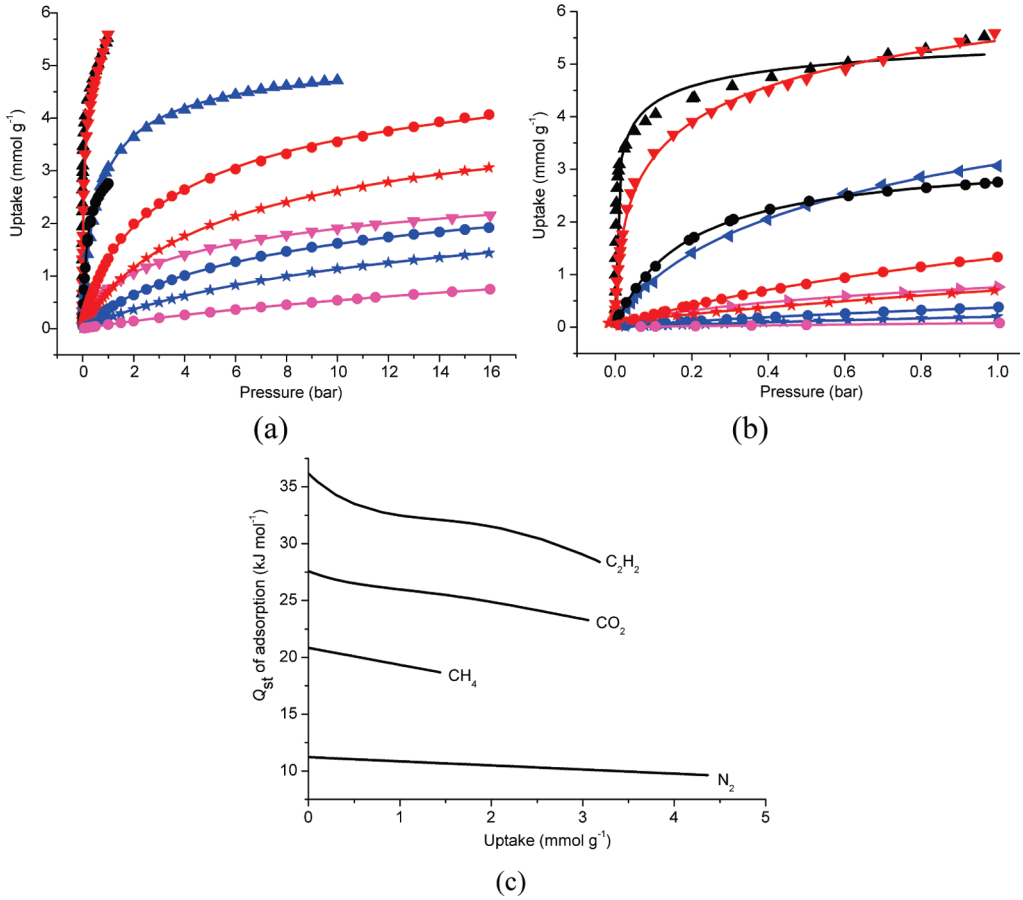

Figure 7. Comparison of gas adsorption on **SOF-1a**. (a) C_2H_2 (black), CO_2 (red), CH_4 (blue), and N_2 (magenta) at 195 K (triangles), 270 (or 273) K (circles) and 298 K (stars). (b) Expanded view of the adsorption isotherms in the low pressure range (0−1 bar). The solid lines are fitted using the Tóth equation. (c) Variation of isosteric heat (Q_{st}) of adsorption with amount of C_2H_2, CO_2, CH_4, and N_2 adsorbed on **SOF-1** (calculated using virial methods).

Clearly, adsorption of CO_2 on **SOF-1a** is markedly greater than that of CH_4 or N_2. At 195 K, the CO_2/CH_4 and CO_2/N_2 ratios of adsorption at pressures below 50 mbar are very high, reaching values of 5−8 and 20−37, respectively. Even at ambient temperature (273 or 298 K), the CO_2/CH_4 and CO_2/N_2 ratios of adsorption are still higher than 2 and 7, respectively, over the pressure range measured, indicating that this material may have practical applications in gas purification. The corresponding Henry's Law selectivity $S_{A/B}$ of gas A (CO_2) over B (CH_4 or N_2) is listed in Table S6.

To further probe the gas affinity of **SOF-1a**, the isosteric heats (Q_{st}) of N_2, CO_2, C_2H_2, and CH_4 adsorption were estimated from the sorption isotherms at various temperatures using virial-type expressions.[22] This confirms (Figure 7c) an order of enthalpy of adsorption at zero coverage of $N_2 < CH_4 < CO_2 < C_2H_2$ (11.2, 20.8, 27.6, and 36.2 kJ mol^{-1}, respectively). The enthalpies of N_2 and CO_2 adsorption for **SOF-1a** suggest that the affinity toward N_2 and CO_2 molecules is in the same range as those observed for many MOF compounds: N_2, 7.68−16 kJ mol^{-1};[23] CO_2, 25−35 kJ mol^{-1}.[24] However, the enthalpy of adsorption observed for methane on **SOF-1a** (20.8 kJ mol^{-1}) is one of the highest values reported so far (*cf* 22 kJ mol^{-1} for microporous polymers and 23 kJ mol^{-1} for PCN-9[3c,25]) and significantly exceeds those of organic microporous crystal of L-alanyl-L-valine (AV) (9 kJ mol^{-1}),[3c] aluminosilicate zeolites (17.0−17.8 kJ mol^{-1}),[26] and other porous metal−organic frameworks (12−17 kJ mol^{-1}).[24,27] The large isosteric heat of adsorption (Q_{st}) for CH_4 observed in **SOF-1a** indicates that although the CH_4 is highly symmetric and nonpolar, some enhancement of binding strength is still possible.[25] The adsorption enthalpy for C_2H_2 at zero coverage ($Q_{st,n=0}$ = 36.2 kJ mol^{-1}) is higher than or comparable with those for previously studied absorbents which generally show values of 28.4−38.5 kJ mol^{-1}.[21b−d] Interestingly, ZIF-8 shows a lower value of 13.3 kJ mol^{-1} at a coverage of 0.02 mmol g^{-1},[21e] while increased values are observed for cucurbit[6]uril (59.4 kJ mol^{-1})[10b] and [Cu_2(pzdc)$_2$(pyz)] (pzdc^{2-} = 2,3-pyrazinedicarboxylate; pyz = pyrazine) (42.5 kJ mol^{-1}).[21a] For **SOF-1a**, as C_2H_2 loading increases, the Q_{st} values decrease gradually to 28.4 kJ mol^{-1} at 3.2 mol g^{-1} loading (Figure 7c).

Conclusions and Perspectives

In summary, we have prepared the multifunctional and multidirectional tecton L^1, and by exploiting the weak cooperative interactions of hydrogen bonds and $\pi-\pi$ stacking interactions, we have successfully obtained a porous organic framework (**SOF-1**) with pyridyl-decorated channels. Desolvated **SOF-1a** exhibits an unusually high thermal stability, and its gas adsorption properties have been investigated. The measurements of uptake of C_2H_2, CO_2, CH_4, and N_2 show a type-I isotherm, but in some cases slight hysteresis was observed on desorption. High C_2H_2 uptake (61 cm^3 g^{-1}) and high C_2H_2/CO_2 (2), C_2H_2/CH_4 (7), C_2H_2/N_2 (36), CO_2/CH_4 (4), CO_2/N_2 (17), and CH_4/N_2 (5) uptake ratios at ambient temperature (270 K for C_2H_2 and 273 K for other gases) and 1 bar are revealed, indicating that **SOF-1a** has potential to emerge as an important material for C_2H_2 and natural gas purification and for removal of CO_2 from the air.

The analogue bis(4-(3,5-dicyano-2,6-dipyridyl)dihydropyridyl)benzene (L^2) has been shown to form two different solvates under the same crystallization conditions; this should be recognized as a potentially complicating but interesting factor in the production of SOFs. Thermal removal of solvents from **S2A** resulted in a conversion to denser phase **S2C** with no effective porosity. Thus, compared with the phenyl analogue (L^2), introduction of 9,10-bis(phenyl)anthracene group (L^1) leads to a stable porous organic material **SOF-1**. The increased role of hydrogen bonding, $\pi-\pi$, hydrophobic, and van der Waals interactions between the walls of the channel host and guest molecules account for the stabilization of **SOF-1**. These interactions will thus be fewer in the **S2** series because of their much smaller spacer group leading to more close-packed structures.

The successful synthesis of stable **SOF-1** opens up the possibility of obtaining new porous materials by using large polyfunctional organic tectons in which a part of cooperative functional groups (i.e., dihydropyridyl and cyano groups in **SOF-1**) stabilizes the supramolecular assembly, while the other polar organic sites (i.e., pyridyl groups in **SOF-1**) remain available for host−guest interactions within decorated pores. To probe this further, we are currently undertaking the challenge of applying core decoration of carboxaldehydes to the synthesis of further functionalized dihydropyridyl derivatives and the formation of their corresponding porous organic assemblies and related polymorphs.

Acknowledgment. We thank EPRSC for support. M.S. gratefully acknowledges receipt of a Royal Society Wolfson Merit Award and of an ERC Advanced Grant.

Supporting Information Available: Experimental details, additional views of the crystal structures, PXRD data, detailed analysis of gas adsorption isotherms analyses, and crystallographic data (in CIF format) for **SOF-1**, **S2A** (both forms), **S2B**, and **S2C**. This material is available free of charge via the Internet at http://pubs.acs.org.

JA1042935

(22) (a) Rowsell, J. L. C.; Yaghi, O. M. *J. Am. Chem. Soc.* **2006**, *128*, 1304. (b) Jagiello, J.; Bandosz, T. J.; Schwarz, J. A. *Langmuir* **1996**, *12*, 2837. (c) Zhao, X. B.; Xiao, B.; Fletcher, A. J.; Thomas, K. M. *J. Phys. Chem. B* **2005**, *109*, 8880. (d) Chen, B.; Zhao, X.; Putkham, A.; Hong, K.; Lobkovsky, E. B.; Hurtado, E. J.; Fletcher, A. J.; Thomas, K. M. *J. Am. Chem. Soc.* **2008**, *130*, 6411. (e) Czepirski, L.; Jagiello, J. *Chem. Eng. Sci.* **1989**, *44*, 797.

(23) (a) Matsuda, R.; Kitaura, R.; Kitagawa, S.; Kubota, Y.; Kobayashi, T. C.; Horike, S.; Takata, M. *J. Am. Chem. Soc.* **2004**, *126*, 14063. (b) Matsuda, R.; Kitaura, R.; Kitagawa, S.; Kubota, Y.; Kobayashi, T. C.; Horike, S.; Takata, M. *J. Am. Chem. Soc.* **2004**, *126*, 14063. (c) Bradshaw, D.; Prior, T. J.; Cussen, E. J.; Claridge, J. B.; Rosseinsky, M. J. *J. Am. Chem. Soc.* **2004**, *126*, 6108. (d) Noro, S.; Kitaura, R.; Kondo, M.; Kitagawa, S.; Ishii, T.; Matsuzaka, H.; Yamashita, M. *J. Am. Chem. Soc.* **2002**, *124*, 2568.

(24) (a) Bourrelly, S.; Llewellyn, P. L.; Serre, C.; Millange, F.; Loiseau, T.; Férey, G. *J. Am. Chem. Soc.* **2005**, *127*, 13519. (b) Loiseau, T.; Lecroq, L.; Volkringer, C.; Marrot, J.; Férey, G.; Haouas, M.; Taulelle, F.; Bourrelly, S.; Llewellyn, P. L.; Latroche, M. *J. Am. Chem. Soc.* **2006**, *128*, 10223.

(25) (a) Ma, S.; Zhou, H.-C. *J. Am. Chem. Soc.* **2006**, *128*, 11734. (b) Ma, S.; Sun, D.; Simmons, J. M.; Collier, C. D.; Yuan, D.; Zhou, H.-C. *J. Am. Chem. Soc.* **2008**, *130*, 1012.

(26) (a) Guillot, A.; Follin, S.; Poujardieu, L. *R. Soc. Chem.−Charact. Porous Solids* **1997**, *213*, 573. (b) Himeno, S.; Komatsu, T.; Fujita, S. *J. Chem. Eng. Data* **2005**, *50*, 369.

(27) (a) Eddaoudi, M.; Kim, J.; Rosi, N.; Vodak, D.; Wachter, J.; OKeeffe, M.; Yaghi, O. M. *Science* **2002**, *295*, 469. (b) Wang, X.-S.; Ma, S.; Rauch, K.; Simmons, J. M.; Yuan, D.; Wang, X.; Yildirim, T.; Cole, W. C.; López, J. J.; de Meijere, A.; Zhou, H.-C. *Chem. Mater.* **2008**, *20*, 3145.